Nanoscale Bending of Multilayered Boron Nitride and Graphene Ribbons: Experiment and Objective Molecular Dynamics Calculations

Ilia Nikiforov, Dai-Ming Tang, Xianlong Wei, Traian Dumitrică, and Dmitri Golberg

Phys. Rev. Lett. **109**, 025504 — Published 11 July 2012

DOI: 10.1103/PhysRevLett.109.025504

Nanoscale Bending of Multilayered Boron Nitride and Graphene Ribbons: Experiment and Objective Molecular Dynamics Calculations

Ilia Nikiforov[1], *Dai-Ming Tang*[2], *Xianlong Wei*[2], *Traian Dumitrică*[1*], *and Dmitri Golberg*[2]

[1]Department of Mechanical Engineering, University of Minnesota, Minneapolis, MN 55455, USA

[2]National Institute for Materials Science, Namiki 1-1, Tsukuba, Ibaraki 305-0044, Japan

PACS: 62.25.-g, 62.23.Kn, 68.27.Lp

By combining experiments performed on nanoribbons *in situ* within a high resolution TEM with objective molecular dynamics simulations, we reveal common mechanisms in the bending response of few-layer-thick hexagonal boron nitride and graphene nanoribbons. Both materials are observed forming localized kinks in the fully reversible bending experiments. Microscopic simulations and theoretical analysis indicate plate-like bending behavior prior to kinking, in spite of the possibility of interlayer sliding, and give the critical curvature for the kinking onset. This behavior is distinct from the rippling and kinking of multi- and single-wall nanotubes under bending. Our findings have implications for future study of nanoscale layered materials, including nanomechanical device design.

* Corresponding author. E-mail: dtraian@me.umn.edu

Recently, there has been an increased interest in understanding the physical properties of multilayered structures of graphene and hexagonal boron nitride (h-BN), such as nanosheets and nanoribbons (NRs).[1-3] A common feature of these materials is that they have a highly anisotropic layered structure. The atoms within individual layers possess strong short-ranged covalent bonding, while the interlayer binding is via comparatively weak long-ranged van der Waals (vdW) forces. Despite the relative weakness of the vdW binding, there is significant energetic advantage in maintaining Bernal stacking where the atoms in sequential layers do not eclipse each other.[4,5]

Often, the more complex multilayered NR structures possess different but similarly fascinating properties than the more-studied single-layer forms.[6,7] For example, in the electronic domain, the three-layered graphene has an intriguing quantum Hall response different from that of the single- and bi-layer graphene.[2] In the mechanical domain, the weak vdW interlayer gluing makes multilayered nanostructures prone to a shear deformation mode[1] in which individual stiff layers glide against each other. It is a priori unclear if graphene and h-BN NRs would respond to mechanical deformation in a plate-like manner, or if the layers tend to slide past each other. A detailed understanding of the consequences of this weak interlayer coupling on the primary mechanical deformation modes is important both for developing applications, and fundamentally, to investigate the validity limits of classical continuum mechanics.

In this Letter, we investigate the bending behavior of graphene (GNRs) and BNNRs via direct bending experiments combined with microscopic simulations. The experimentation is enabled by our capability to both synthesize NRs of each type and directly manipulate nanostructures *in-situ* within a high-resolution TEM.[3,8] We demonstrate that both nanomaterials show remarkable resilience against mechanical manipulation. Rather than fracturing, they bend reversibly and form localized kinks. On the theoretical side, there are difficulties associated with simulating bending, as this deformation breaks the

commonly employed translational symmetry. We are able to reveal the mechanisms involved by atomistic simulations performed with objective molecular dynamics (MD). Our method allows us to impose pure bending deformations via angular objective boundary conditions, which contrast to the traditional translational-only periodic boundary conditions.[9] Because kinking is caused by the severe compression of the inner layers, bending of both graphene and h-BN is plate-like, with no layer sliding occurring.

The NRs used in our experiments were picked up under HRTEM imaging of synthetic powders, which mostly contained the corresponding multiwalled nanotubes (MWNTs). The nanotubes (NTs) were produced at high yields using so-called boron oxide assisted CVD procedure (BN) and an arc-discharge technique (C). The NRs were by-products of the respective syntheses. The number of layers in the NRs used in our experiments ranged from 9 to 13. The mechanical tests reported here were performed inside a 300 kV high-resolution field emission TEM (JEM 3100FEF) equipped with a state-of-art sample STM-TEM holder (Nanofactory Instruments) with a piezo-tube driven manipulator. A chemically etched W nanoprobe was mounted onto the manipulator to act as a movable probe that can be driven in 3D with nearly nanometer precision under the piezo-tubes' drives. The NRs were attached to the edge of a counterpart Au wire, which was set onto the fixed terminal facing the W probe. Under TEM observations, individual NRs protruding from the Au wire edge were firstly selected, and their structure was entirely characterized using high-resolution TEM imaging and electron diffraction. Under the control of the manipulator, the W nanoprobe was moved to contact with the free end of a NR.

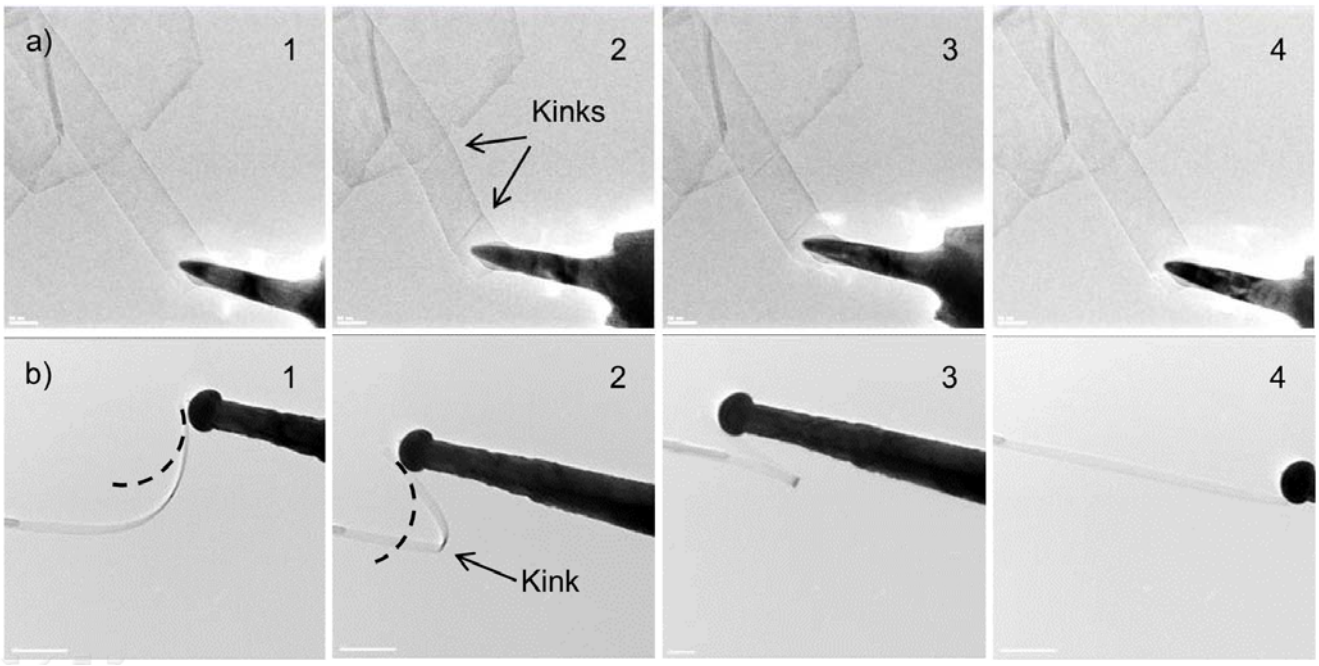

Figure 1. a) Bending (1,2) and recovery (2,3) cycle of 12-layer BNNR. Scale bars are 50 nm. Width is 82 nm, length is ≈300 nm. b) Bending (1-3) and recovery (4) cycle of 9-layer GNR, showing critical curvature for kinking predicted from simulations (dotted line). Scale bars are 100 nm. Width is 34 nm, length is ≈500 nm.

Both materials exhibited localized kinking under bending, as shown for a 12-layer BNNR in Fig. 1a and a 9-layer GNR in Fig. 1b. The bending process is fully reversible, with the NRs returning to a pristine straight state when unloaded. Very little deformation is required to initiate kinking. In the case of a very long and flexible NR, as the 9-layer 500 nm-long GNR seen in Fig 1b, a smooth bending stage can be observed prior to kinking. The curvature range in which kinking initiates is in agreement with our computational predictions. The morphology of the kink area further emerges from the HRTEM image presented in Fig. 2, where the characteristic dark fringes indicate the wrinkling of the constituent layers. The atomistic details of the morphology leading to these fringes were uncovered in our simulations, Fig. 3a.

What is the underlying mechanism leading to kinking? When considering the pure bending of graphene and h-BN, two contrasting mechanisms are conceivable: plate-like bending, where the layers bend collectively and do not slide relative to each other, or a mechanism where layer sliding occurs. One can identify these mechanisms by simply bending a stack of paper. On one hand, in the plate-like case there is an invariant neutral surface, on the opposite sides of which there is extension and compression of the constituent layers. On the other hand, bending accompanied by layer sliding efficiently releases these in-plane strains on both sides of the neutral surface. Only in the first case would the compression of the inner layers cause them to wrinkle and a kink to arise. Thus, the occurrence of kinking itself, as well as the layer wrinkling seen in Fig. 2, are indications that bending in graphene and h-BN commences in a plate-like manner.

Relying on the above arguments, we performed simulations of the bending process using objective MD. The method implicitly constrains the system to plate-like bending.[10] We performed pure bending simulations of h-BN and graphene sections with a length of 10 nm in the bending direction. Up to 10 layers were considered, with simulation cells containing between 320 and 1600 atoms. Only bending in the zigzag direction was considered, as graphene and h-BN in-plane behavior is nearly isotropic at low strains.[11,12] The synthesized NRs have widths of tens of nanometers, or hundreds of atomic distances, and the experimental load is applied directly along the length, so the finite width of the NRs should have little effect. Thus, although the simulations represent an infinite plate, they can be accurately applied to the NR experiments. Various degrees of bending were applied to the simulation cell by varying the curvature in steps of at most 1 deg/nm of tube length. In order to prevent the simulation from getting trapped in metastable states, MD was performed to randomize the configuration at each step, followed by energy minimization. This protocol has previously been successful in simulating bending of nanotubes[13] and, indeed, the energy graphs (Fig. 3b) show that the transition between smoothly bent

and kinked states does not show any energy discontinuity – the simulation relaxes to the lowest energy configuration. The covalent interatomic interactions within the layers were described here with the Tersoff potential [14], a many-body potential widely used for studying deformations of graphitic structures. For B-N we use the parameters of Verma et al.[15] The long-range interlayer interactions were accounted for with a standard Lennard-Jones potential. The parameters for graphene ($\epsilon = 2.39$ meV, $\sigma = 3.41$ Å) were the well-proven parameters of Girifalco et al.,[16] while the parameters for h-BN ($\epsilon = 5.0$ meV, $\sigma = 3.35$ Å) were fitted by us to match the interlayer spacing and binding energy obtained from the recent dispersion-corrected DFT calculations of Maromet et al.[5] Note that the interlayer binding in BN is approximately twice as strong as in graphene.

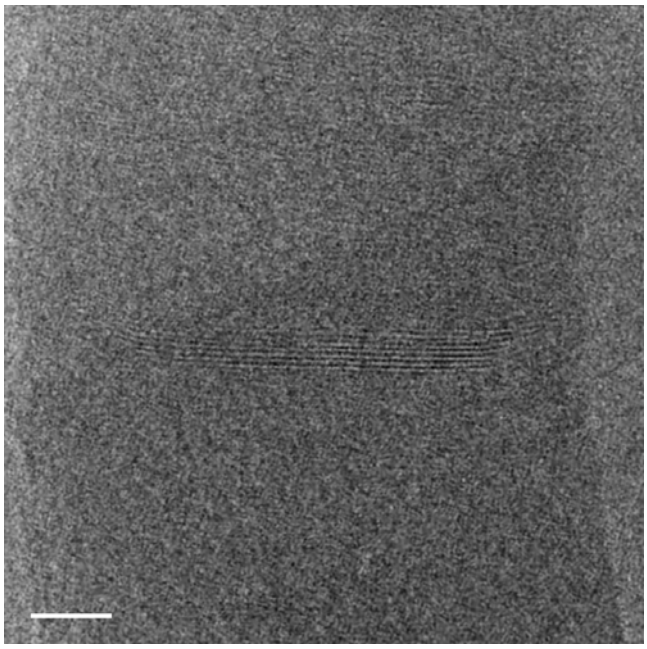

Figure 2. Kink developed in 9-layer GNR. This HRTEM image was taken towards the end of the bending stage (different experiment than Fig. 1b). It shows typical dark fringes, the cause of which is shown in Fig. 3a. Scale bar is 5 nm.

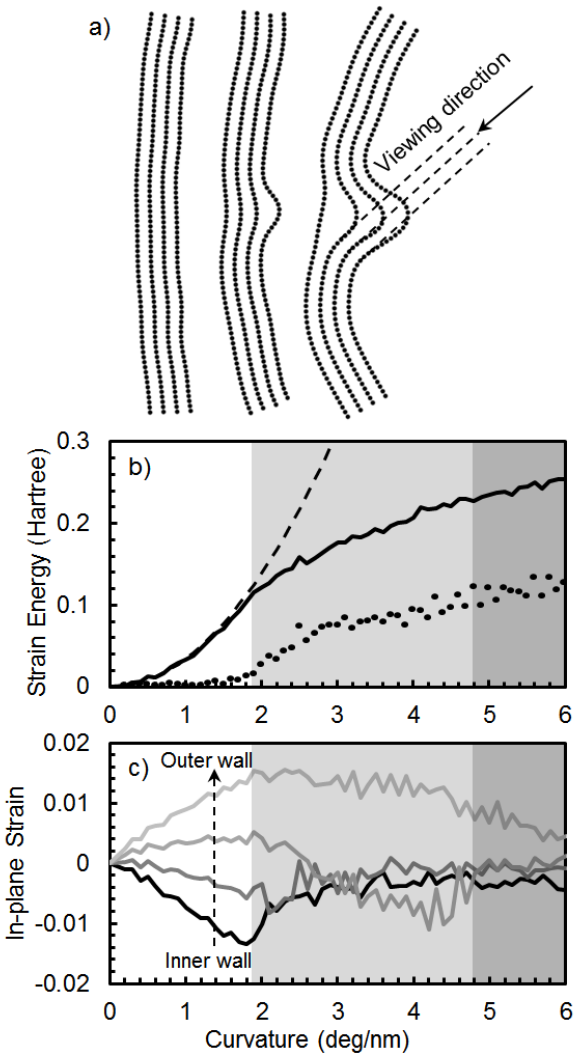

Figure 3. Objective MD simulations for the bending of 4-layer h-BN. Three stages are indicated – (i) ideal plate-like (no layers wrinkled – unshaded on graphs), (ii) intermediate (some layers wrinkled – shaded light gray) and (iii) final (only outer layer not wrinkled – shaded dark gray). a) Morphology, revealing the origin of the dark fringes seen in the TEM Figure 2. b) Energy – dashed line indicates plate behavior as described by ref. [10], solid line indicates total bending energy, dotted line indicates interlayer vdW component. c) In-plane strain in individual layers.

Fig. 3 shows the a) morphologies, b) energetics and c) the individual layers' in-plane strain, characteristic of *all* the bending simulations, using the example of 4-layer h-BN. We display the bending

strain energy, as well as the interlayer vdW energy component. The in-plane strain was defined as the fractional difference between the deformed and original length of each layer in the bending direction. Bending of NRs is characterized by three stages. (i) At first the bending is smooth in all layers (Fig 3a, left), and the strain energy closely follows the finite-size-corrected plate model of Zhang et al.,[10] using the in-plane Young's modulus of the appropriate set of Tersoff potential (Fig. 3b). The energy depends quadratically on the curvature and the coefficient scales as the cube of the number of layers, N^3. This strain energy is due to the compression of the inner layers and the elongation of outer layers (Fig. 3c), i.e. plate-like behavior. The vdW component of the strain energy is negligible during the smooth-bending stage. (ii) At the critical curvature κ_{cr}, the inner layer wrinkles (Fig. 3a, middle). The vdW component becomes non-negligible due to the layer spacing becoming non-optimal at the kink, and the total strain energy begins to fall off from the plate model (Fig. 3b). (iii) As the curvature increases, the wrinkling propagates to inner layers until only the outermost layer is not wrinkled (Fig. 3a, right). From Fig. 3c it can be seen that after each layer kinks, it quickly returns to its undeformed length, releasing *all* compressive strain. This behavior is in agreement with previous literature on wrinkling of layered structures.[17] The tensile strain in the outer layers, meanwhile, is released by the movement of the entire simulation cell towards the rotation axis, slightly increasing the curvature.

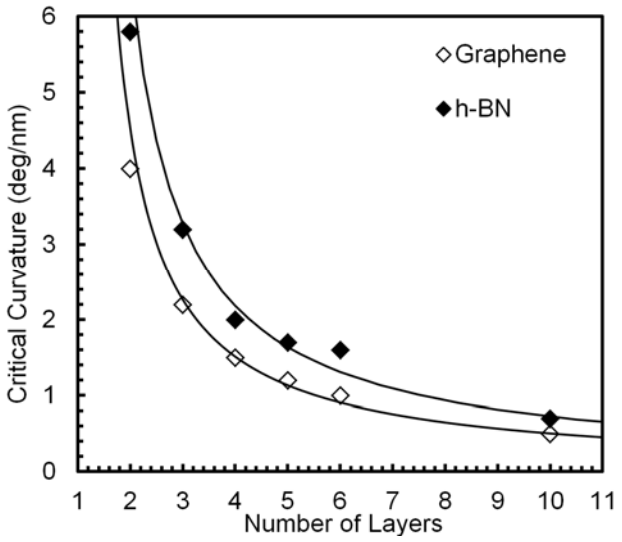

Figure 4. Critical curvatures for kinking. Continuous lines show fitting with eq. 1 using B=6.6 and 4.53 deg/nm for graphene and h-BN, respectively.

Our simulation results are in good agreement in all important respects with the experimental behavior, indicating that the above microscopic picture may be used to predict the kinking behavior of NRs. Broadly, we predict that both graphene and h-BN should demonstrate kinking at very small deformations, as seen in the experiments. The kinking morphology seen in the simulations is consistent with the dark fringes seen in HRTEM images of kinks, while the lack of bond-breaking in the simulations is consistent with the reversibility of the bending in the experiments. The experiment shown in Fig. 1b lends itself to direct quantitative comparison to the simulations because a smooth bending stage can be observed before kinking. Additionally, the length and flexibility of this GNR means that the deformation is nearly pure bending.

We now give the dependence of the critical curvature for kinking κ_{cr} on the number of layers N. As simulations suggest, the compression of the inner layer is the key cause of kinking. This allows us to assume that kinking begins at a fixed material-specific critical stress σ_{cr} in the innermost layer. In the

simplified Euler-Bernoulli case, the in-plane stress at distance d from the neutral axis is $\sigma_{cr} \propto \kappa_{cr} d$. For the most inner layer $d \propto N-1$, thus

$$\kappa_{cr} = \frac{B}{N-1}, \qquad (1)$$

where B is a proportionality constant. Note that this simplified model precludes any length-dependence. To verify this, we performed a full range of simulations on graphene, using 5 nm-long simulation cells. Indeed, reducing the length by a factor of 2 caused only a 10% increase in critical curvature, showing that the length-dependence is secondary. Fig. 4 displays the critical curvature found from each of our simulations as well as the fitting of eq. 1, using B=6.6 and 4.5 deg/nm, for BN and graphene, respectively, meaning that graphene kinks $\approx$150% earlier. The differences in the elastic properties of the h-BN and graphene monolayers are too small to account for this. Thus, this dissimilarity in B is largely due to the stronger interlayer binding in h-BN – it is more energetically expensive to disturb the perfect interlayer spacing by creating a wrinkle in h-BN than it is in graphene. The dotted lines in Fig. 1b show the critical curvature as predicted by eq. 1, allowing us to test its validity. The curvature range in which the GNR kinks agrees with this prediction.

It is instructive to compare these results with the behavior of NTs under bending. Unlike multilayered NRs, MWNTs with closed cores feature complex competing forces when they bend. While the compression of the inner side of the bend still drives localized bending of the walls, the core of the NT provides support and prevents deep kinks from forming. Because of this, MWNTs tend to form distributed ripples at intermediate curvatures.[13,17] Additionally, in MWNTs, there is circumferential stress arising from these competing forces, while in multilayered NRs, there is no in-plane stress perpendicular to the bending direction.[17] Conceptually, the bending of single-wall NTs (SWNTs) and MWNTs with open cores is closer to the bending of NRs. The lack of support from a closed core causes

a localized kink to form under bending, similar to NRs.[13,18] However, the circumferential connection between the inner and outer bending surface still plays a role. Due to this, both MWNTs and SWNTs show a $\kappa_{cr} \propto 1/R^2$ dependence of the critical curvature κ_{cr} on the tube radius R, in contrast to the $\kappa_{cr} \propto 1/R^2$ dependence on the thickness T we observe in NRs.[13,18]

In summary, direct bending experiments show that BNNRs and GNRs tend to bend reversibly by forming a localized kink, caused by the wrinkling of individual layers. The kinking behavior observed is universal despite the much more complex interlayer binding in h-BN compared to graphene.[4,5] Simulations reveal the atomistic details of bending, which is smooth and plate-like at low curvatures, followed by kinking, the morphology and mechanics of which are in agreement with our experiments. Kinking occurs at lower curvatures for graphene than h-BN due to the stronger interlayer binding in the latter material. By examining the atomistic details of kinking, we proposed a simple model to predict the critical curvature at which kinking begins in experiment. The kinking behavior of the NRs was found to be significantly different from that of MW- and SWNTs. Our model can be used to predict the behavior of graphene and h-BN nanoribbons and nanosheets under bending in future experiments, as well as aid in the design of nanomechanical devices. The common bending behavior revealed here likely extends to even more complex layered materials of current interest, such as MoS_2.[19]

[1] P. H. Tan, W. P. Han, W. J. Zhao*, et al*, Nature Mater. **11**, 294 (2012).

[2] E. A. Henriksen, D. Nandi, and J. P. Eisenstein, Phys. Rev. X **2**, 011004 (2012).

[3] H. Zeng, C. Zhi, Z. Zhang, X. Wei, X. Wang, W. Guo, Y. Bando, and D. Golberg, Nano Lett. **10**, 5049 (2010).

[4] A. Carlson and T. Dumitrică, Nanotechnology **18**, 065706 (2007).

[5] N. Marom, J. Bernstein, J. Garel, A. Tkatchenko, E. Joselevich, L. Kronik, and O. Hod, Phys. Rev. Lett. **105**, 046801 (2010).

[6] K. S. Novoselov, A. K. Geim, S. V. Morozov, D. Jiang, Y. Zhang, S. V. Dubonos, I. V. Grigorieva, and A. A. Firsov, Science **306**, 666 (2004).

[7] K. K. Kim, A. Hsu, X. Jia*, et al*, Nano Lett. **12**, 161 (2012).

[8] X. Bai, D. Golberg, Y. Bando, C. Zhi, C. Tang, M. Mitome, and K. Kurashima, Nano Lett. **7**, 632 (2007).

[9] T. Dumitrică and R. D. James, J. Mech. Phys. Solids **55**, 2206 (2007).

[10] D. - B. Zhang, E. Akatyeva, and T. Dumitrică, Phys. Rev. Lett. **106**, 255503 (2011).

[11] H. Zhao, K. Min, and N. R. Aluru, Nano Lett. **9**, 3012 (2009).

[12] J. Song, J. Wu, Y. Huang, and K. C. Hwang, Nanotechnology **19**, 445705 (2008).

[13] I. Nikiforov, D. - B. Zhang, R. D. James, and T. Dumitrică, Appl. Phys. Lett. **96**, 123107 (2010).

[14] J. Tersoff, Phys. Rev. B **39**, 5566 (1989).

[15] V. Verma, V. K. Jindal, and K. Dharamvir, Nanotechnology **18**, 435711 (2007).

[16] L. A. Girifalco, M. Hodak, and R. S. Lee, Phys. Rev. B **62**, 13104 (2000).

[17] L. Mahadevan, J. Bico, and G. McKinley, Europhys. Lett. **65**, 323 (2004).

[18] S. Iijima, C. Brabec, A. Maiti, and J. Bernholc, J. Chem. Phys. **104**, 2089 (1996).

[19] J. Brivio, D. T. L. Alexander, and A. Kis, Nano Lett. **11**, 5148 (2011).